J. Synchrotron Rad. (2000). **7**, 152–159

Anomalous X-ray scattering for determining the partial structural functions of binary liquids

Masatoshi Saito* and Yoshio Waseda

Institute for Advanced Materials Processing (AMP), Tohoku University, Sendai 980-8577, Japan. E-mail: masaito@iamp.tohoku.ac.jp

(*Received 31 January 2000; accepted 23 February 2000*)

The availability of intense white X-rays from synchrotron radiation sources has greatly improved both acquisition and quality of anomalous X-ray scattering (AXS) measurements. A demonstration is given of the usefulness of the AXS method for determining three partial structural functions of liquid matter by some selected examples of molten salts such as CuBr and RbBr.

Keywords: partial structure factors; anomalous X-ray scattering; reverse Monte Carlo simulations; molten CuBr; molten RbBr.

1. Introduction

The liquid state of matter has recently received attention from both the points of view of basic and applied science because of the novelty of the physics involved, mainly arising from the particular non-periodicity in the atomic arrangements. Part of the reason for this is that liquid-state physics seems to have made slow progress among the three typical states of matter: solid, liquid and gas. This has led to an increasing need for determining liquid structure accurately at a microscopic level.

Quantitative description of the microscopic structure of liquids usually employs the so-called radial distribution function (RDF). The environment of each atom in non-crystalline systems including more than two components generally differs from that of other atoms. This makes the interpretation of their RDFs not so easy. In addition, the structure–property relationships of multicomponent non-crystalline systems can be discussed only when the full set of partial RDFs for the individual chemical constituents are provided. Thus, the utmost importance of the determination of partial structural functions is well recognized as one of the most essential research subjects for non-crystalline systems including more than two components (*e.g.* Waseda *et al.*, 1992). However, the actual implementation of this subject is not a trivial task even for binary liquids.

Several techniques have been developed to determine the partial structure factors, corresponding to the Fourier transform of RDFs. For example, the partial structure factors for a binary system can be estimated by making available at least three independent intensity measurements for which the weighting factors are varied without any change in their atomic distribution. The isotope substitution method for neutron diffraction, firstly applied by Enderby *et al.* (1966) to liquid Cu–Sn alloys and to several molten salts (Page & Mika, 1971), is considered undoubtedly one of the most powerful methods. However, it seems intrinsically to be somewhat limited in practice by availability of suitable isotopes and the structure is automatically assumed to remain identical upon substitution by the isotopes. The use of anomalous X-ray scattering near the absorption edge of the constituent elements (hereafter referred to as AXS) (Waseda, 1984) will, in the present author's view, bring about a significant breakthrough in such difficulties without any assumption for many more elements in the periodic table. The availability of intense white X-rays from synchrotron radiation sources has greatly improved both acquisition and quality of the AXS data by enabling the use of an energy in which the anomalous X-ray scattering effect is the greatest.

The main purpose of this work is to demonstrate the usefulness of the AXS method for determining the partial structural functions with two selected examples: molten CuBr and RbBr. A new apparatus suitable for AXS measurements of high-temperature liquids is also included.

2. Fundamentals for the AXS method

The method for analysing the measured AXS intensity data for liquids has already been described in detail (Ramesh & Ramaseshan, 1971; Waseda, 1984) so only some essential points are given below. The partial structure factor of the i–j pair, $a_{ij}(Q)$, in the Faber–Ziman form (Faber, 1972), is connected with the partial pair distribution function $g_{ij}(r)$ by the Fourier transformation in the following equation,

$$a_{ij}(Q) = 1 + (4\pi\rho_0/Q)\int_0^\infty r\,[g_{ij}(r) - 1]\sin(Qr)\,\mathrm{d}r, \qquad (1)$$

where ρ_0 is the average number density in the system. The so-called reduced interference function, $i(Q,E)$, for a binary liquid can be described as follows, using the coherent X-ray scattering intensity $I(Q,E)$, corresponding

to the structurally sensitive part of the total scattering intensity,

$$i(Q,E) \equiv I(Q,E) - \sum_i c_i f_i{}^2(Q,E) = \sum_{i=1}^{2}\sum_{j=1}^{2} c_i c_j f_i(Q,E) f_j(Q,E)\big[a_{ij}(Q) - 1\big], \quad (2)$$

where Q and E are the wavevector and the incident X-ray energy, respectively, c_i is the atomic fraction, $f_i(Q,E)$ is the atomic scattering factor of the i component. The coefficients of $[a_{ij}(Q) - 1]$ in (2) are known to depend on the concentrations and the atomic scattering factors. Then, the individual partial structure factors, $a_{ij}(Q)$, can be estimated from three independent intensity measurements for which the coefficients are altered. The utilization of the anomalous dispersion effect is one way of varying the atomic scattering factors in these coefficients, because a distinct energy dependence due to the anomalous dispersion effect clearly appears in the close vicinity of the absorption edge relevant to *K*- or *L*-shell electrons of a constituent, as exemplified by Fig. 1 using the results of Fe, Co and Zn. In such an energy region the atomic scattering factor should be given by

$$f(Q,E) = f^0(Q) + f'(E) + if''(E), \quad (3)$$

where $f^0(Q)$ corresponds to the scattering factor of the atom at an energy sufficiently away from the absorption edge, and $f'(E)$ and $f''(E)$ are the real and imaginary parts of the anomalous dispersion terms.

The solid lines in Fig. 1 show the anomalous dispersion factors of Fe, Co and Zn (Waseda, 1984) theoretically calculated by the relativistic Cromer–Liberman scheme (Cromer & Liberman, 1970) together with the values of Zn experimentally determined from the absorption coefficient measurement for crystalline $ZnFe_2O_4$ (Shinoda *et al.*, 1995). The theoretical values do not coincide with the experimental ones at the higher-energy side because of the presence of the phenomena of extended X-ray absorption fine structure (EXAFS) and the X-ray absorption near-edge structure (XANES), as well as the large background by the fluorescent radiation at the higher-energy side. Furthermore, it is rather worth mentioning that the value of $f'(E)$ shows a drastic change at the lower-energy side of the absorption edge, whereas the value of $f''(E)$ and its energy variation is quite small in this energy region. For these reasons a large change of $f'(E)$ at the lower-energy side of the absorption edge is employed in the present AXS method.

When the incident X-ray energy is tuned in to the lower-energy side of the absorption edge $E_{\rm abs}$ of a specific element, for example A in the A–B binary system, the anomalous dispersion effect becomes significantly detected, and thereby the variation between intensities, $\Delta i_A(Q, E_1, E_2)$, measured at the incident energies of E_1 and E_2, is attributed to only a change in the real part of anomalous dispersion terms of the component A. Then, the following relation can readily be obtained,

$$\Delta i_A(Q,E_1,E_2) \equiv \frac{[I(Q,E_1) - \langle f^2(Q,E_1)\rangle] - [I(Q,E_2) - \langle f^2(Q,E_2)\rangle]}{c_A[f'_A(E_1) - f'_A(E_2)]W(Q,E_1,E_2)} = \frac{c_A \mathrm{Re}\,[f_A(Q,E_1) + f_A(Q,E_2)]}{W(Q,E_1,E_2)}[a_{AA}(Q) - 1] + \frac{c_B \mathrm{Re}\,[f_B(Q,E_1) + f_B(Q,E_2)]}{W(Q,E_1,E_2)}[a_{AB}(Q) - 1], \quad (4)$$

$$W(Q,E_1,E_2) = \sum_{k=A,B} c_k \mathrm{Re}\,[f_k(Q,E_1) + f_k(Q,E_2)], \quad (5)$$

where $E_{\rm abs} > E_2 > E_1$ and Re denotes the real part of the values in the brackets. The quantity $\Delta i_A(Q, E_1, E_2)$ contains two partial structure factors, $a_{AA}(Q)$ and $a_{AB}(Q)$ in an A–B binary system. Similarly, $\Delta i_B(Q, E_3, E_4)$ includes $a_{BB}(Q)$ and $a_{AB}(Q)$. Then, for obtaining the three partial structure factors, the following set of equations should be solved,

$$\begin{pmatrix} \Delta i_A(Q,E_1,E_2) \\ \Delta i_B(Q,E_3,E_4) \\ i(Q,E_5) \end{pmatrix} = \begin{pmatrix} c_A\mathrm{Re}[f_A(Q,E_1) + f_A(Q,E_2)]/W(Q,E_1,E_2) & c_B\mathrm{Re}[f_B(Q,E_1) + f_B(Q,E_2)]/W(Q,E_1,E_2) & 0 \\ 0 & c_A\mathrm{Re}[f_A(Q,E_3) + f_A(Q,E_4)]/W(Q,E_3,E_4) & c_B\mathrm{Re}[f_B(Q,E_3) + f_B(Q,E_4)]/W(Q,E_3,E_4) \\ c_A^2 f_A^2(Q,E_5) & 2c_A c_B f_A(Q,E_5) \times f_B(Q,E_5) & c_B^2 f_B^2(Q,E_5) \end{pmatrix} \times \begin{pmatrix} a_{AA}(Q) - 1 \\ a_{AB}(Q) - 1 \\ a_{BB}(Q) - 1 \end{pmatrix} \quad (6)$$

where the ordinary term, $i(Q, E_5)$, is obtained at the energy E_5, far from the absorption edges of both components of A and B.

The following two advantages may be stressed with respect to the AXS measurements, especially for liquids: (i) the weighting factors can be varied without the use of different samples; (ii) a liquid sample is often contained in a cell with windows transparent for X-rays and then the intensity from a liquid sample alone must be estimated by accurately correcting the scattering intensity from the window materials. This is usually carried out using the intensity only from the window materials corrected for absorption by the liquid sample (Saito, Park, Omote *et al.*, 1997). With respect to this point, the AXS intensity profiles measured at E_2 and E_1 contain the contribution from the window materials as well as from the sample liquid. However, when taking a difference between the two

profiles at E_2 and E_1, the contribution from the window materials as well as that from the none-A pairs is automatically eliminated. In this way we are released from the tedious correction procedure for the window materials.

3. Experimental

The AXS measurements were carried out with synchrotron radiation at beamlines of stations 6B and 7C (Nomura *et al.*, 1991) of the Photon Factory, Institute of Materials Structure Science, High Energy Accelerator Research Organization, Tsukuba, Japan. A monochromatic incident X-ray beam at energies ranging from 4 to 21 keV was obtained with an Si(111) double-crystal monochromator. The scattering intensities were measured by an Si(Li) solid-state detector so that the fluorescent radiation from the sample in the measurement near the absorption edge can be removed from the elastic scattering with a pulse-height analyser. The measurements were made in the transmission mode for molten CuBr with a devised quartz cell and in the asymmetrical reflection mode for molten RbBr with a beam-direction-changing mirror system. The number densities ρ_0 of the molten CuBr at 810 K and RbBr at 960 K are 36.3 nm^{-3} and 19.7 nm^{-3}, respectively (Janz, 1967). The detailed experimental procedures are described elsewhere (Saito, Park, Omote *et al.*, 1997; Saito, Park, Sugiyama *et al.*, 1997). Only some essential points are given below.

3.1. *Transmission mode*

Fig. 2(*a*) shows a schematic diagram of the experimental set-up in the transmission mode using the devised quartz cell. For example, the molten CuBr sample was filled in a cell through tubes with a spacing of 50 μm sandwiched between two windows (10 mm × 20 mm and thickness 100 μm). The optimum sample thickness (50 μm in the present case) was determined from a condition that the scattered intensity has to be sufficiently secured and the absorption is not too strong. The sample was heated at a temperature of 810 K in a purified nitrogen atmosphere. It may be suggested that the sample reservoir was encased with nickel for trapping CuBr vapour from the reservoir. This sample cell was positioned in a high-temperature chamber.

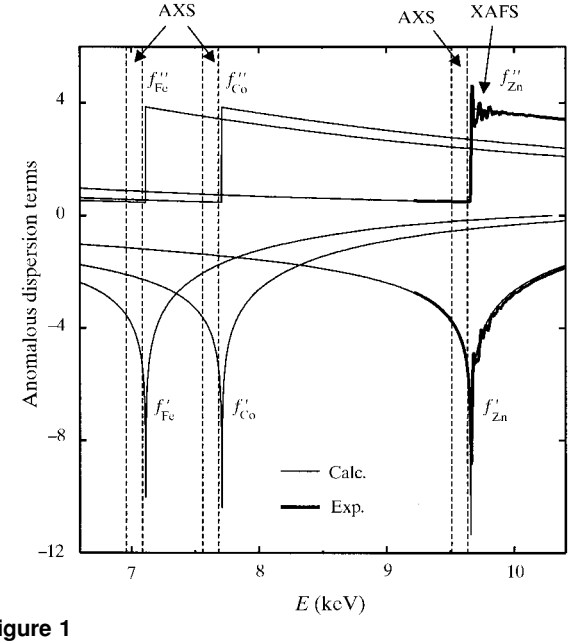

Figure 1
Energy variations of anomalous dispersion factors for Fe, Co and Zn in the close vicinity of their respective K-absorption edge, as calculated by the relativistic Cromer–Liberman method. The experimental data of Zn are taken from the results of Shinoda *et al.* (1995).

3.2. *Reflection mode*

Fig. 2(*b*) shows the case of the (asymmetrical) reflection mode for a free surface of high-temperature liquids using a glancing-angle control system. For convenience, the schematic X-ray optics is also given in Fig. 3. A monochromatic horizontal X-ray beam is first diffracted downward through a Bragg angle $2\varphi(E)$ by a W/Si multilayer mirror ($2d$ = 4.05 nm). The multilayer mirror is set on a stage which rotates in order to adjust the angle φ and translates along a translation stage (length 600 mm). The translation stage itself is also mounted on the arm of a separate rotation axis, the 2φ axis. The individual rotation axis of φ and 2φ and the translation stage are synchronously controlled, so that the X-ray beam diffracted by the W/Si multilayer mirror passes just through the centre of the 2φ axis. In this configuration the change of the beam direction by the multilayer mirror is redirected by the translation such that it is always incident at the centre of the spectrometer (the right of Fig. 2*b*). The beam is then totally reflected by the flat fused quartz mirror coated with Pt with adjustable reflection angle ω, which is mounted at the centre. Throughout a specific X-ray energy region this mirror system can keep the final emitted beam direction constant; that is, a glancing angle α is fixed. The W/Si multilayer mirror always faces downwards. It is suggested that the Pt-coated mirror can face upwards when $2\varphi(E)$ is larger than α and downwards when $2\varphi(E)$ is smaller than α. If the critical angle for the total reflection from the Pt-coated mirror, $2\omega_c(E)$, is larger than $|2\varphi(E) - \alpha|$, it is possible to adjust the final emitted beam direction without any significant loss of intensity.

The high-temperature chamber is mounted on the centre of the double-axis diffractometer (the left side in Fig. 2). The molten RbBr sample was heated up to a temperature of 960 K in a rectangular platinum crucible (30 mm × 10 mm and depth 3 mm) under a purified nitrogen atmosphere.

4. Two selected examples of binary liquids by applying the AXS method

4.1. *Partial structural functions of molten CuBr*

Fig. 4 gives the environmental interference functions of molten CuBr at 810 K, $Q\Delta i_{Cu}(Q)$ for Cu and $Q\Delta i_{Br}(Q)$ for Br, which are obtained from the measurements at incident

energies of 8.680, 8.955, 13.170 and 13.445 keV. These four energies correspond to 300 and 25 eV below the Cu K (8.980 keV) and Br K (13.470 keV) absorption edges, respectively. The anomalous dispersion terms for Cu and Br for these energies are listed in Table 1. The normal atomic scattering factors are taken from the compilation of *International Tables for X-ray Crystallography* (Wilson, 1995). The ordinary interference function $Qi(Q)$ estimated from the scattering profile at the single energy of 17.0 keV is also illustrated in this figure.

Fig. 5 shows the three partial structure factors $a_{ij}(Q)$ of molten CuBr, where the vertical lines denote the uncertainty estimated from the experimental data by solving the simultaneous linear equation of (3). The numerical solutions of the simultaneous linear equations appear to be ill-conditioned at several Q values, giving some physically unreasonable behaviour in the resultant radial distribution functions. Such behaviour is mainly due to the experimental uncertainty caused from the relatively small difference between the anomalous dispersion terms at the two energies and the unpredictably large fluctuation in the numerical solution of equation (3) when the pivot of the matrix is close to zero (Stantson, 1961). At the present time, such small experimental errors cannot always be avoided. However, the reverse Monte Carlo (hereafter referred to as RMC) simulation technique (McGreevy & Pusztai, 1988) might be one way to reduce this inconvenience. For this reason we employed the RMC method along the way essentially identical to that described by McGreevy & Pusztai (1988) with an initial configuration of 1728 particles in a cubic box of size L = 3.624 nm. Three calculated interference functions were compared with the experi-

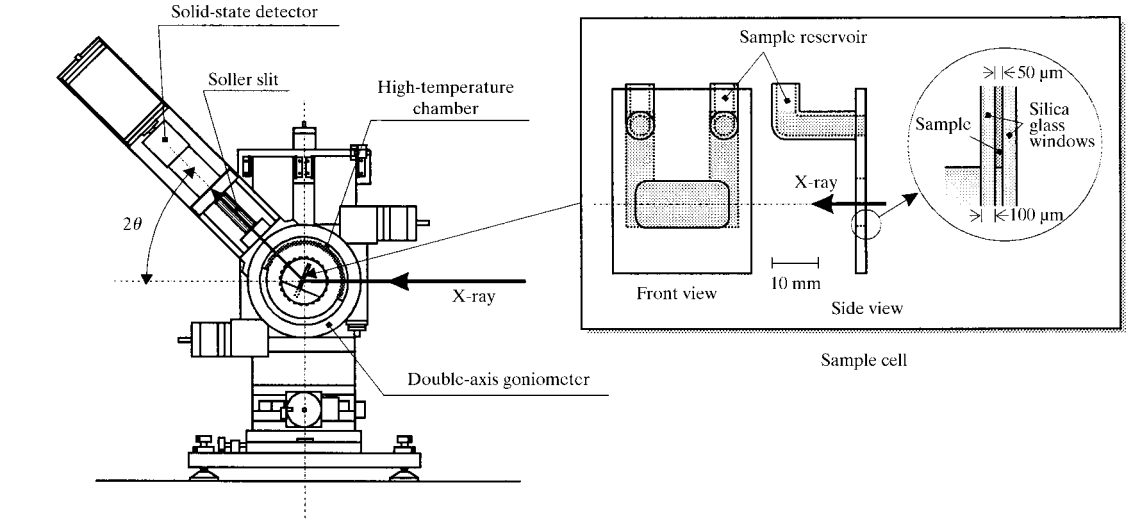

(*a*)

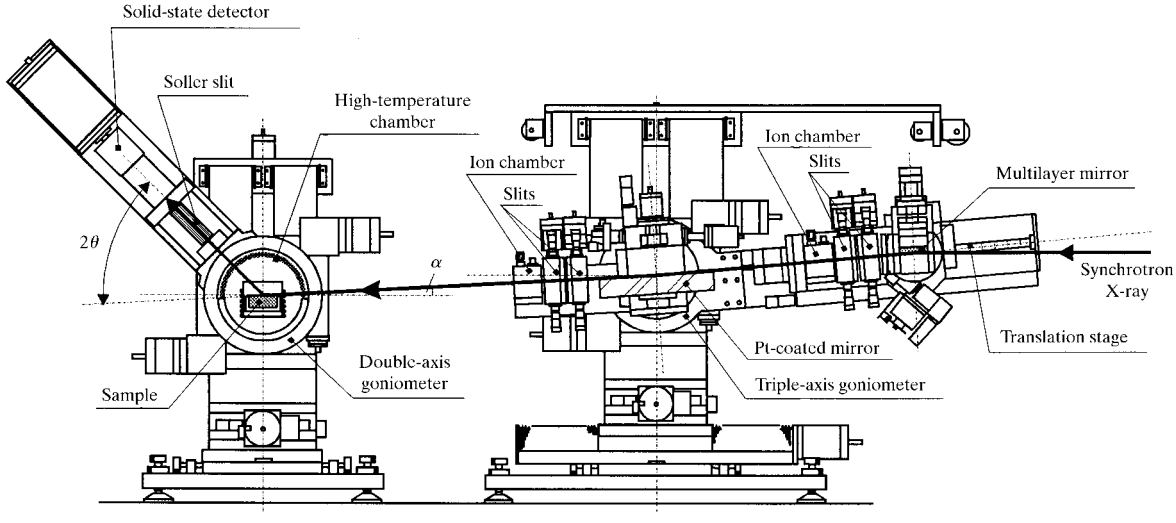

(*b*)

Figure 2
Schematic diagram of the experimental set-up for the AXS measurements in (*a*) the transmission mode with a devised quartz cell and (*b*) the reflection mode from a free surface by changing the beam direction using an additional mirror system.

Table 1
Anomalous dispersion terms for Cu, Rb and Br used in this work.

Energy	Cu		Rb		Br	
8.680 keV (Cu K −300 eV)	$f' = -3.06$	$f'' = 0.51$	–	–	$f' = -0.90$	$f'' = 1.12$
8.955 keV (Cu K −25 eV)	$f' = -5.58$	$f'' = 0.49$	–	–	$f' = -0.96$	$f'' = 1.06$
13.170 keV (Br K −300 eV)	$f' = 0.00$	$f'' = 2.06$	$f' = -1.79$	$f'' = 0.66$	$f' = -3.37$	$f'' = 0.53$
13.445 keV (Br K −25 eV)	$f' = 0.04$	$f'' = 1.99$	$f' = -1.90$	$f'' = 0.64$	$f' = -5.82$	$f'' = 0.51$
14.902 keV (Rb K −300 eV)	–	–	$f' = -3.47$	$f'' = 0.53$	$f' = -1.21$	$f'' = 3.19$
15.177 keV (Rb K −25 eV)	–	–	$f' = -5.91$	$f'' = 0.51$	$f' = -1.40$	$f'' = 3.10$
17.0 keV	$f' = 0.26$	$f'' = 1.33$	$f' = -1.29$	$f'' = 3.11$	$f' = -0.48$	$f'' = 2.57$

mental results and such a comparison was continued with further iteration until a reasonable convergence was obtained, so as to reproduce the three independent interference functions $Q\Delta i_{Cu}(Q)$, $Q\Delta i_{Br}(Q)$ and $Qi(Q)$ (dotted lines in the Fig. 4). The resultant partial structure factors obtained by the RMC simulation technique are illustrated by the solid lines in Fig. 5. The partial structure factors determined through this procedure with the RMC simulation are considered to be the least conditions necessary for explaining the three independent experimental results of Fig. 4, although they might not be sufficient conditions for a full explanation. The agreement between the present AXS results for molten CuBr with those obtained by neutron diffraction with isotope substitution (Allen & Howe, 1992) are, in the present author's view, rather surprisingly good. The profiles of $a_{BrBr}(Q)$ and $a_{CuBr}(Q)$ are found to be very similar to those of simple ionic liquids such as molten alkali halides, by observing that the first valley of $a_{CuBr}(Q)$ is located at a Q value where the principal peak in $a_{BrBr}(Q)$ is situated. In contrast, the partial structure factor of $a_{CuCu}(Q)$ for cation–cation pairs was found to be rather structureless, similar to that found in molten CuCl (Page & Mika, 1971; Eisenberg *et al.*, 1982).

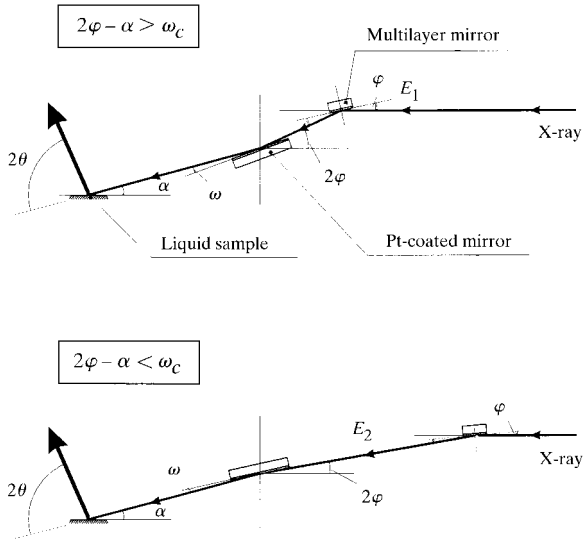

Figure 3
Schematic diagram of the X-ray optics in the reflection mode using a W/Si multilayer mirror and a flat fused quartz mirror coated with Pt.

The resultant partial pair distribution functions $g_{ij}(r)$ of molten CuBr are given in Fig. 6. The closest Cu—Cu distance is significantly smaller than that for the Br—Br pair, indicating the like-ion penetration into the first unlike-ion coordination shell. This characteristic penetration may be interpreted by a decrease in the Coulombic repulsion force interacting between Cu ions arising from the reduced charge transfer between unlike ions. The peak positions in $4\pi r^2\rho_0 g_{ij}(r)$ and the coordination numbers N_{ij} defined by the integration of $4\pi r^2\rho_0 g_{ij}(r)$ up to the first minimum are estimated and the results are summarized in Table 2, together with the values of the corresponding crystalline phase of γ-CuBr (ZnS-type structure) (Bührer & Hälg, 1977). The coordination numbers for Br—Br pairs are found to be 11.4 at a distance of 0.398 nm. These values are not far from the crystalline case. The coordination numbers for Cu—Br pairs are found to be 3.1 at a distance of 0.245 nm in the liquid state. When considering a perfect f.c.c. lattice of anions, the coordination numbers N_{+-} of anions around a cation located at an octahedral site and

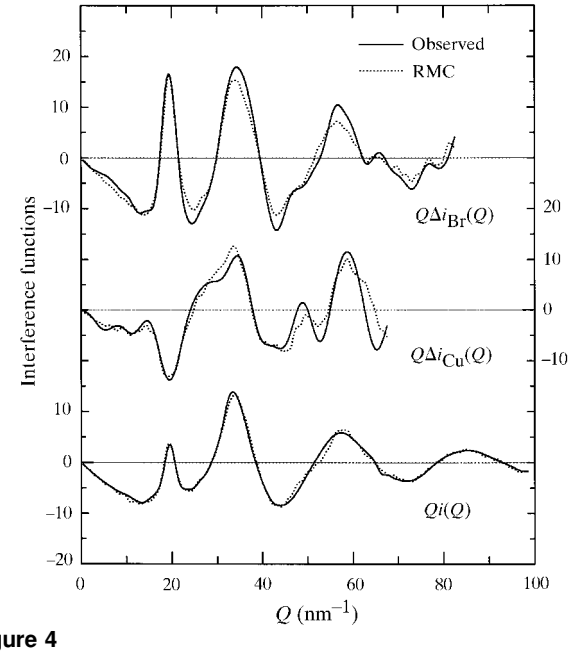

Figure 4
The ordinary interference function $Qi(Q)$ and the environmental interference functions $Q\Delta i_{Cu}(Q)$ and $Q\Delta i_{Br}(Q)$ of molten CuBr at 810 K. Solid lines correspond to the experimental data. Dotted lines denote values calculated by the RMC method.

tetrahedral one is six with $r_{--}/r_{+-} = 1.41$ and four with $r_{--}/r_{+-} = 1.63$, respectively. In the molten state the coordination number might be decreased by thermal agitation. The value of r_{--}/r_{+-} for molten CuBr is 1.62, which is not far from that of the tetrahedral position. Thus, the present authors maintain the view that the structure of molten CuBr can be a disordered close packing of anions where the Cu ions take strongly disordered distribution by meandering through essentially tetrahedral holes.

4.2. *Partial structural functions of molten RbBr*

Fig. 7 gives the environmental interference functions of molten RbBr at 960 K, $Q\Delta i_{\mathrm{Br}}(Q)$ for Br and $Q\Delta i_{\mathrm{Rb}}(Q)$ for Rb, which are obtained from the measurements at incident energies of 13.170, 13.445, 14.902 and 15.177 keV. These four energies correspond to 300 and 25 eV below the Br K and Rb K (15.202 keV) absorption edges, respectively. The anomalous dispersion terms used for Rb are also listed in Table 1. The ordinary interference function $Qi(Q)$ obtained using the single energy of 17.0 keV is also given in this figure.

Fig. 8 shows the three partial structure factors of molten RbBr obtained by using the RMC method similar to in the CuBr case. For the RMC simulation we used a configuration of 4096 atoms (2048 atoms represent Rb and the remaining atoms represent Br) in a cubic box of size L = 5.924 nm. The partial structure factors of $a_{\mathrm{RbRb}}(Q)$ and $a_{\mathrm{BrBr}}(Q)$ are very similar, suggesting that cations and anions behave in an almost identical way, although appreciable difference is noted between the ionic radii of Rb^+ (0.148 nm) and Br^- (0.195 nm). For the cross correlation, $a_{\mathrm{RbBr}}(Q)$ has a deep valley at the same Q value as that of the principal peaks in $a_{\mathrm{RbRb}}(Q)$ and $a_{\mathrm{BrBr}}(Q)$.

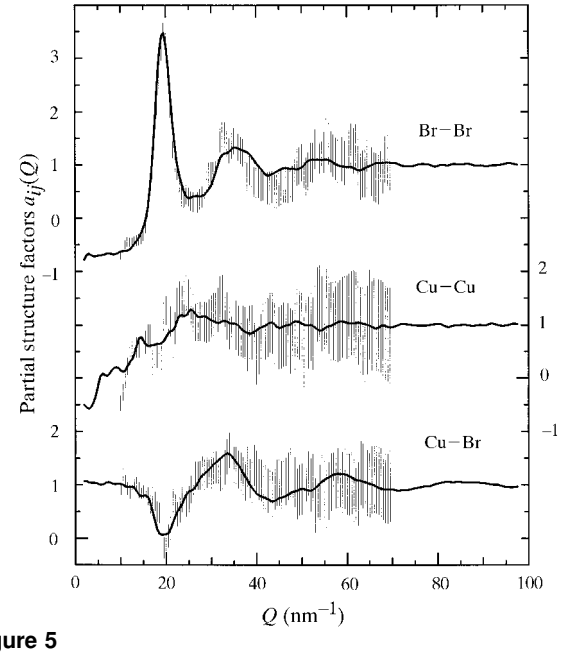

Figure 5
Three partial structure factors of molten CuBr at 810 K. Solid lines correspond to the values calculated by the RMC method.

The resultant partial pair distribution functions $g_{ij}(r)$ of molten RbBr are shown in Fig. 9. It can be found that $g_{\mathrm{RbRb}}(Q)$ and $g_{\mathrm{BrBr}}(Q)$ are approximately in anti-phase with $g_{\mathrm{RbBr}}(Q)$, indicating well defined charge ordering. The peak positions and the coordination numbers are also listed in Table 2, together with the values of the corresponding crystalline phase of NaCl-type structure. The coordination numbers for unlike-ion and like-ion pairs are estimated to be 5.4 and ~13.6, respectively. Although the nearest-neighbour distance for the Rb—Br pair decreases on

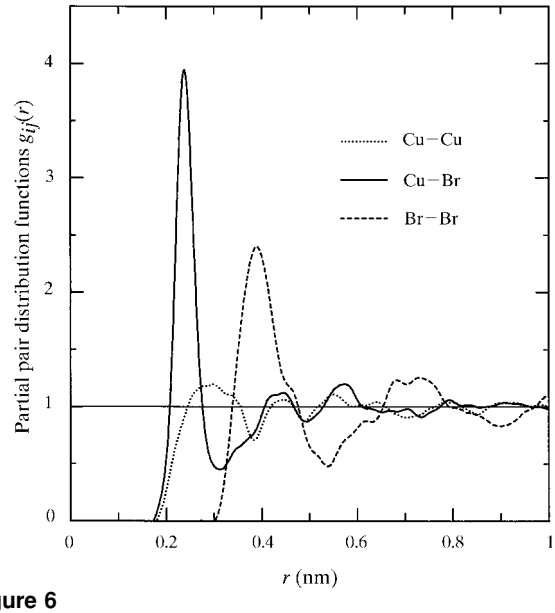

Figure 6
Three partial pair distribution functions of molten CuBr at 810 K.

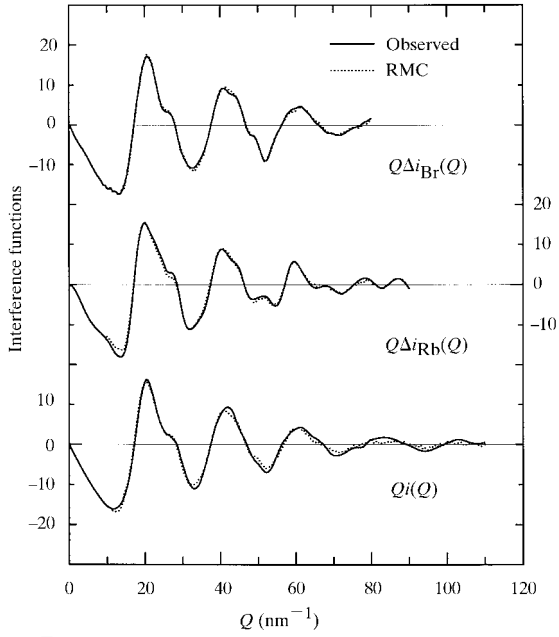

Figure 7
The ordinary interference function $Qi(Q)$ and the environmental interference functions $Q\Delta i_{\mathrm{Rb}}(Q)$ and $Q\Delta i_{\mathrm{Br}}(Q)$ of molten RbBr at 960 K. Solid lines correspond to the experimental data. Dotted lines denote values calculated by the RMC method.

Table 2
Summary of structural parameters in molten CuBr and RbBr.

	Molten CuBr (810 K)				Molten RbBr (960 K)					
	Cu—Br		Br—Br		Rb—Rb		Rb—Br		Br—Br	
	r_{+-} (nm)	N_{+-}	r_{--} (nm)	N_{--}	r_{+-} (nm)	N_{+-}	r_{+-} (nm)	N_{+-}	r_{--} (nm)	N_{--}
Present work	0.245 ±0.003	3.1 ±0.3	0.398 ±0.003	11.4 ±0.4	0.495 ±0.003	13.5 ±0.5	0.337 3 ±0.00	5.4 ±0.3	0.484 ±0.003	13.7 ±0.5
Crystalline state	0.247	4	0.403	12	0.501	12	0.354	6	0.501 2	1
r_{--} / r_{+-}	1.62				1.44					

melting, the variation in the first coordination number is rather small, close to that of the crystalline state. It may be added that the ratio of r_{--}/r_{+-} for molten RbBr is 1.44 which is closer to the octahedron value of 1.41. Fig. 10 illustrates a representative ionic configuration generated by the RMC method for molten RbBr. The $RbBr_6$ units are selected and drawn as octahedra in this figure. It can be seen that octahedral configurations for the nearest-neighbour Rb—Br pair are predominant in the molten state. Considering all the results, it is safe to suggest that the symmetrical first coordination shell of the Rb—Br pair can be described by the octahedral configuration, as it is in the crystalline state. These structural features are quite similar to the case for molten alkali chlorides (*e.g.* Mitchell *et al.*, 1976), whose quantitative accuracy is well appreciated.

5. Concluding remarks

The capability of the anomalous X-ray scattering (AXS) method has been well recognized by obtaining the partial structural functions of a binary liquid, although the insufficient absolute accuracy of the experimental data still prevents us from obtaining exact direct solutions of the simultaneous linear equations from the AXS measurements alone. The reverse Monte Carlo simulation technique appears to provide one useful way of reducing such inconvenience. As well as the transmission mode using a devised quartz cell, the present results clearly show that the reflection mode of the AXS measurement from a free liquid surface with the synchrotron radiation source could also be realized with a triple-axis spectrometer utilizing the combination of a W/Si multilayer mirror and a flat fused quartz mirror coated with Pt. It should be noted here that the apparatus with the reflection mode may show its ability fully for liquids which have larger mass absorption coefficients (*e.g.* liquid metals and alloys) since the transmission geometry is impractical in these cases.

The partial structural functions for molten CuBr and RbBr given in this work provide a step forward for obtaining a direct link between the atomic scale structure and characteristic liquid properties. Thus, it would be quite interesting to extend the AXS measurements to the determination of the partials in many liquid systems. It may also be worth mentioning that many numerical data on the structure of liquids and anomalous dispersion factors with

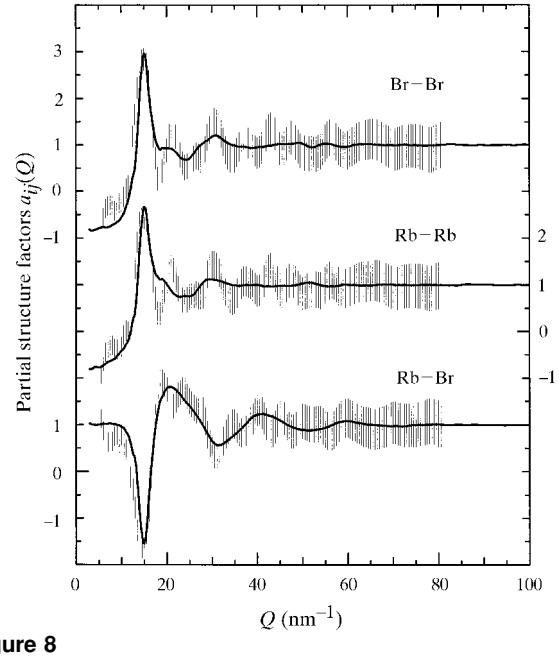

Figure 8
Three partial structure factors for molten RbBr at 960 K. Solid lines correspond to the values calculated by the RMC method.

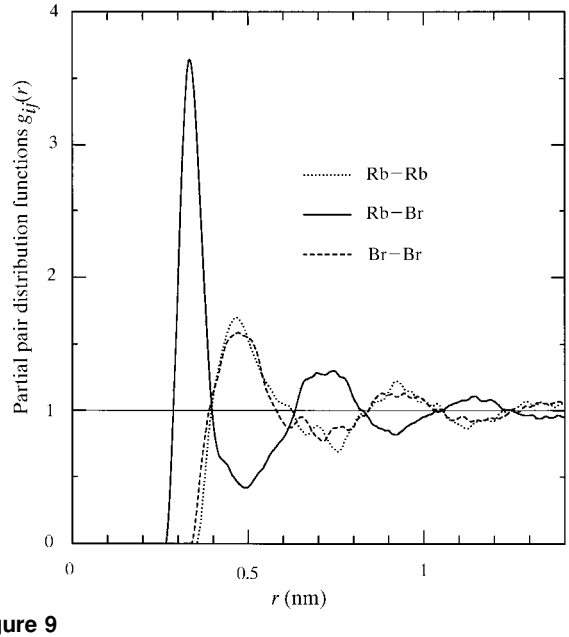

Figure 9
Three partial pair distribution functions for molten RbBr at 960 K.

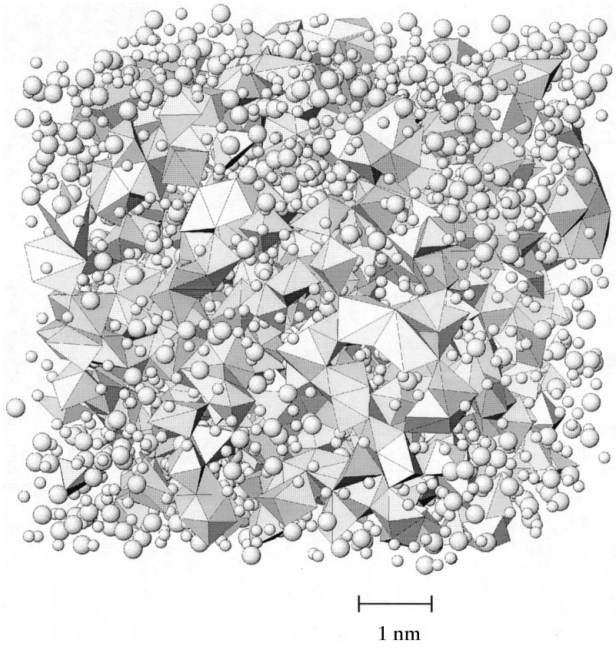

Figure 10
A section of the atomic positions from a representative RMC-generated configuration for molten RbBr. Larger atoms are Br, smaller atoms are Rb. $RbBr_6$ units are selected and drawn by octahedra.

linear absorption coefficients of almost all elements as a function of energy are available in our public database (SCM-AXS) given at http//www.iamp.tohoku.ac.jp.

The authors wish to express their gratitude to Professor M. Nomura, Photon Factory, Institute of Materials Structure Science, High Energy Accelerator Research Organization, for his help on the AXS measurements (Proposal No. 97-G213).

References

Allen, D. A. & Howe, R. A. (1992). *J. Phys. Condens. Matter*, **4**, 6029–6038.
Bührer, W. & Hälg, W. (1977). *Electrochim. Acta*, **22**, 701–706.
Cromer, D. T. & Liberman, D. A. (1970). *J. Chem. Phys.* **53**, 1891–1898.
Eisenberg, S., Jal, S. F., Dupuy, J., Chieux, P. & Knoll, W. (1982). *Philos. Mag.* A**46**, 195–209.
Enderby, J. E., North, D. M. & Egelstaff, P. A. (1966). *Philos. Mag.* **14**, 961–970.
Faber, T. E. (1972). *An Introduction to the Theory of Liquid Metals.* Cambridge University Press.
Janz, G. J. (1967). *Molten Salt Handbook.* New York: Academic Press.
McGreevy, R. L. & Pusztai, L. (1988). *Mol. Simul.* **1**, 359–367.
Mitchell, E. W. J., Poncet, P. F. J. & Stewart, R. J. (1976). *Philos. Mag.* **34**, 721–732.
Nomura, M., Koyama, A. & Sakurai, M. (1991). KEK Report 91–1. National Laboratory for High Energy Physics, Tsukuba, Japan.
Page, D. I. & Mika, I. (1971). *J. Phys.* C**4**, 3034–3044.
Ramesh, T. G. & Ramaseshan, S. (1971). *J. Phys.* C**4**, 3029–3033.
Saito, M., Park, C., Omote, K., Sugiyama, K. & Waseda, Y. (1997). *J. Phys. Soc. Jpn*, **66**, 633–640.
Saito, M., Park, C., Sugiyama, K. & Waseda, Y. (1997). *J. Phys. Soc. Jpn*, **66**, 3120–3126.
Shinoda, K., Sugiyama, K. & Waseda, Y. (1995). *High Temp. Mater. Process.* **14**, 75–79.
Stantson, R. G. (1961). *Numerical Methods for Science and Engineering.* New York: Prentice Hall.
Waseda, Y. (1984). *Novel Application of Anomalous X-ray Scattering for Structural Characterization of Disordered Materials.* New York: Springer-Verlag.
Waseda, Y., Matsubara, E., Okuda, K., Omote, K., Tohji, K., Okuna, S. N. & Inomata, K. (1992). *J. Phys. Condens. Matter*, **4**, 6355–6366.
Wilson, A. J. C. (1995). Editor. *International Tables for X-ray Crystallography*, Vol. C. Dordrecht: Kulwer.